Turkish Journal of Electrical Engineering & Computer Sciences

http://journals.tubitak.gov.tr/elektrik/

Research Article

Turk J Elec Eng & Comp Sci
(2019) 27: 4596 – 4607

doi:10.3906/elk-1904-6

Computation of stability regions for load frequency control systems including incommensurate time delays

Şahin SÖNMEZ*
Department of Electrical and Electronics Engineering, Faculty of Engineering,
Niğde Ömer Halisdemir University, Niğde, Turkey

Received: 01.04.2019 • **Accepted/Published Online:** 27.06.2019 • **Final Version:** 26.11.2019

Abstract: This article studies the impact of incommensurate communication time delays on stability regions defined in proportional-integral (PI) controller parameter space for a two-area load frequency control (LFC) system. Distributed power generations and large power plants increase the complexity and control issues of interconnected power systems. In interconnected power systems, LFC systems need to have complex communication networks to exchange data between control center and geographically dispersed generations. The receiving/transmitting of remote measuring data through communication infrastructures causes inevitable time delays, which adversely affect controller performance and stability of the LFC system. Time delays introducing feedback control loops of a multiarea LFC system could exhibit incommensurate characteristics. In this study, a simple graphical method based on extracting a stability boundary locus is implemented to get PI controller parameters responsible for stabilizing the LFC system having incommensurate delay values. The boundaries of the stability regions in the PI controller parameter space are confirmed by time-domain simulations and a numerical algorithm known as the quasipolynomial mapping-based root finder algorithm. Results illustrate that incommensurate delays have remarkable effects on the stability region.

Key words: Incommensurate time delays, stability region, PI controller design, load frequency control systems

1. Introduction

This study aims to compute all proportional-integral (PI) controller gains constituting a region in the parameter space of the controller for a conventional two-area load frequency control (LFC) system with constant incommensurate communication delays. In an interconnected power system, when sudden changes in load demands are experienced, each generating unit is equipped with LFC systems to restore the frequency and to maintain power exchange among control areas at the scheduled value [1]. Wide-area measurement/monitoring systems (WAMSs) comprise extensively open and distributed communication networks that cause unavoidable time delays in electrical power systems [2], particularly in LFC systems. The task of communication networks is to transmit real-time measurement data using synchronous phasor measurement units and global positioning systems from power plants to control centers or vice versa. However, time delays observed because of the complex communication networks and digital measuring devices cause a poor dynamic performance of the controller and have an adverse effect on the dynamics and stability of the LFC system [3–6].

Remote measuring data obtained from WAMSs must be transmitted to a control center at long distances through open and distributed communication networks. Then the control signals for the regulating of the system

*Correspondence: sahinsonmez@ohu.edu.tr

frequency must be transmitted to power plants at remote. However, the communication signals for each control area of the LFC system might have incommensurate time delays due to many reasons such as geographical location of the distributed power system areas, technical specifications of communication technologies and networks, or long distances between control centers and power plants. The incommensurate time delays are introduced to the feedback control loop of each control area in the LFC system. It was reported that communication delays observed in LFC systems are generally in the range of 5–15 s [7].

Many research studies on delay-dependent stability analysis of LFC systems have been presented in the literature. These studies mainly compute the stability delay margin considering incommensurate or commensurate time delays such that two-area LFC systems with time delay for any given PI controller parameters will be at least marginally stable. In order to calculate delay margins of time-delayed LFC systems, time-domain and frequency-domain approaches are commonly used. The frequency-domain approaches aim to find critical eigenvalues or roots of the system [8–12]. The indirect time-domain methods are based on the Lyapunov stability theory and linear matrix inequality techniques [4,13–15]. For given PI controller gains, these methods could effectively calculate stability delay margins. However, whenever the PI controller parameters are retuned or changed, one of the important issues for these methods is that one needs to check the stability and determine the stability delay margin, causing time-consuming stability checks. In order to avoid such a time-consuming stability check and hence to save tuning time of the controller, it is essential to obtain all possible stabilizing PI controller gain values ensuring a stable operation of the LFC system for a finite time delay.

This paper proposes a simple and efficient analytical method to determine all stabilizing PI controller parameter values that constitute a stability region of an LFC system in controller parameter space. The approach is based on the stability boundary locus that can be easily determined by equating real and imaginary parts of the characteristic equation to zero [16,17]. The proposed method has been efficiently applied to the computation of the traditional PI controller [18], fractional-order PD controller of time-delayed systems [19], PI controller synthesis for wind turbine systems [20], and PI controller synthesis of microgrid systems with time delay [10]. Due to uncertainties and perturbations in the controller parameters, some studies to evaluate system performance focus on fragility analysis for any PI controller gains inside stability regions obtained using different methods [21,22]. In our previous studies, the proposed method was used to compute the stability regions for a single-area LFC system with time delay [23,24] and the gain-phase margins-based stability regions of an LFC system whose control areas included identical time delays [25]. Unlike the identical time delay case for each control loop [25], this study considers that each feedback control loop has a different time delay value, especially incommensurate delays. This is a more realistic approach in LFC systems in which control signals could be transmitted to control areas in different delay values. Therefore, the impact of the incommensurate delays on the stability regions must be exhaustively investigated. The first main contribution of this work is the identification of all possible stabilizing PI controller parameters for the two-area LFC system for various incommensurate delay scenarios. Moreover, the consideration of incommensurate time delays in each control loop of the LFC system could provide more flexibility compared to [25] in the stability regions as it evidently makes it possible to investigate the impact of different time delay scenarios on the size and shape of stability regions.

Finally, the accuracy of the stability boundary locus determined by the proposed graphical method is validated by the quasipolynomial mapping-based root finder (QPmR) algorithm [26] and time-domain simulations [27], which is the second main contribution of this work. The QPmR algorithm computes the quasipolynomial spectrum (zeros) over large regions of the complex plane. The algorithm was efficiently used in many research

studies [28,29].

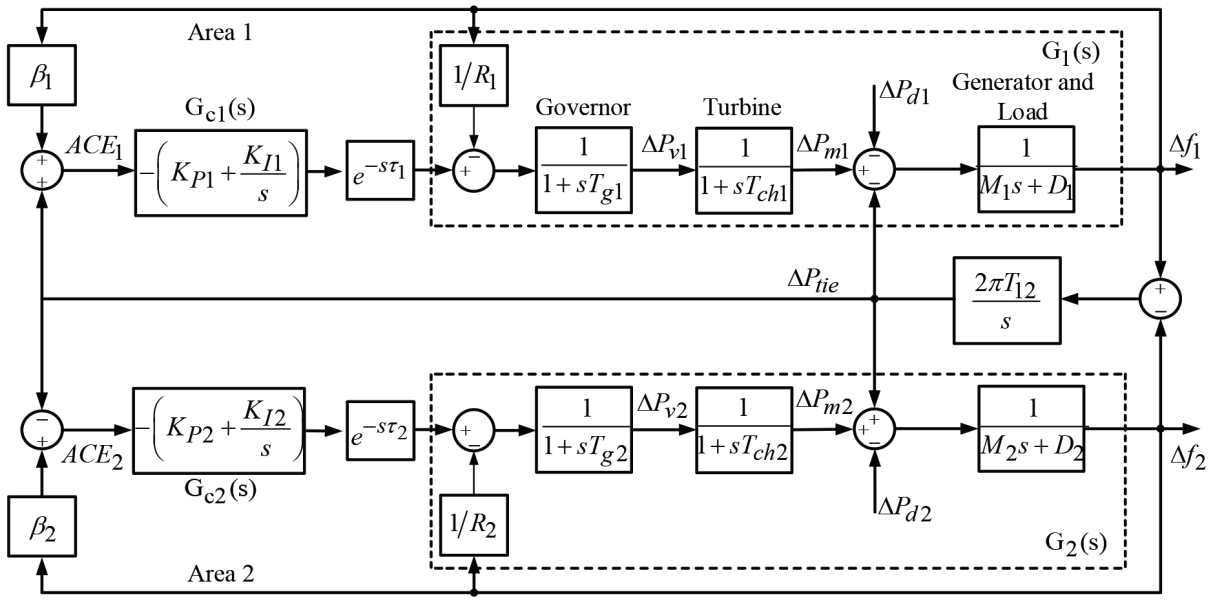

Figure 1. The LFC system model including incommensurate communication time delays.

2. Conventional two-area LFC system model

Figure 1 shows the conventional two-area LFC system model with incommensurate time delays into feedback loops. Here, the traditional LFC system is modified to include incommensurate time delays (τ_1, τ_2). In Figure 1, ΔP_m, ΔP_d, Δf, and ΔP_v are the mechanical output of the generator, control area load, deviation in the frequency, and the valve position, respectively. T_g, T_{ch}, T_{12}, M, D, R, and β represent the time constant of the governor and turbine, tie-line synchronizing power coefficient between area 1 and area 2, inertia constant, damping coefficient, speed drop of each control area, and frequency bias factor, respectively. The PI controller gains are assumed to be identical in each control area, $K_{P1} = K_{P2} = K_P$ and $K_{I1} = K_{I2} = K_I$. Finally, ACE represents the area control error of each control area. As shown in Figure 1, due to exponential terms, ACE is transmitted as a delayed signal for each control loop of the LFC system.

The usage of open communication networks leads to two types of time delays in feedback control loops of LFC systems. These delays are known as controller-to-plant and sensor-to-controller delays. Sensor-to-controller delay is defined as measuring the time delay between power system sensing devices and the controller at a remote control center. Controller-to-plant delay is defined as time delay observed between the control center and power generation units. The control center side is assumed to wait for reception of the remote measuring signal data. The consideration is identical for each delay case. Consequently, such delays are aggregated into a single delay from the control center [3,7]. Many research studies have mostly used the aggregation approach for stability analysis of time-delayed LFC systems [3,14,30]. In Figure 1, τ_1 and τ_2 are incommensurate constant time delays and represent the total amount of controller-to-plant and sensor-to-controller delay in each control area. These delay terms are modeled as exponential transfer functions of $e^{-s\tau_1}$ and $e^{-s\tau_2}$ in Figure 1. In order to

obtain the stability regions, the characteristic equation of the time delayed LFC system is required [6]:

$$\Delta(s,\tau_1,\tau_2) = a_0(s) + a_{11}(s)e^{-s\tau_1} + a_{12}(s)e^{-s\tau_2} + a_2(s)e^{-s(\tau_1+\tau_2)} = 0, \tag{1}$$

where $a_0(s)$, $a_{11}(s)$, $a_{12}(s)$, and $a_2(s)$ are polynomials in s and their coefficients depend on parameters of the LFC system's PI controller. The degrees of these polynomials with real coefficients are 9, 6, 6, and 3, respectively, for the two-area LFC system shown in Figure 1.

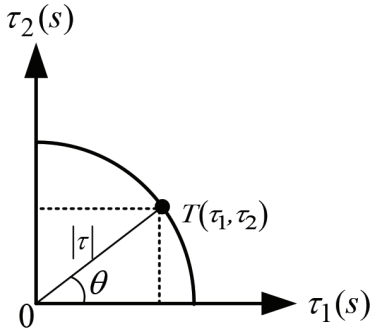

Figure 2. Changing of τ_1 and τ_2 time delay values in a direction.

3. Computation of stability regions

3.1. Selection of incommensurate delays

The incommensurate time delays τ_1 and τ_2 are expressed in polar coordinate $(\theta, |\tau|)$ as shown in Figure 2. All points are defined as $T(\tau_1,\tau_2)$ on a boundary depending on $(\theta, |\tau|)$ in τ_1- and τ_2-space. Magnitude $|\tau|$ and angle θ are defined as $|\tau| = \sqrt{\tau_1^2+\tau_2^2}$ and $\theta = \tan^{-1}(\tau_2/\tau_1)$ [13,14]. By changing the angle in a range of $\theta \in [0^0 - 90^0]$ while magnitude $|\tau|$ is kept constant, the polar coordinate representation of the time delays (τ_1 and τ_2) will enable us to investigate the impact of different cases such as $\tan\theta = \tau_2/\tau_1 < 1$ for $\theta \in [0^0 - 45^0)$, $\tan\theta = \tau_2/\tau_1 = 1$ for $\theta = 45^0$, and $\tan\theta = \tau_2/\tau_1 > 1$ for $\theta \in (45^0 - 90^0]$. To investigate the effect of incommensurate delay cases on the stability regions, three different cases could be considered for a specified $|\tau|$: i) Case 1: Delay in area 1 is greater than that of area 2 ($\tau_1 > \tau_2$), ii) Case 2: Delay in area 1 is equal to that of area 2 ($\tau_1 = \tau_2$), and iii) Case 3: Delay in area 1 is less than that of area 2 ($\tau_1 < \tau_2$).

3.2. Computation of stability regions of the LFC system with incommensurate time delays

In this section, all possible stabilizing PI controller parameters (K_P, K_I) of the two-area LFC system for three different delay cases mentioned are determined. Note that (K_P, K_I) gains need to be extracted from (1) for the computation of stability regions. Therefore, the characteristic equation in (1) is rearranged as follows:

$$\Delta(s,\tau_1,\tau_2) = M(s) + P(s)(K_P s + K_I) + R(s)(K_P s + K_I)^2 = 0, \tag{2}$$

where:

$M(s) = a_0(s) = m_9 s^9 + m_8 s^8 + m_7 s^7 + m_6 s^6 + m_5 s^5 + m_4 s^4 + m_3 s^3 + m_2 s^2$,

$P(s) = \left(p_{15}s^5 + p_{14}s^4 + p_{13}s^3 + p_{12}s^2 + p_{11}s\right)e^{-s\tau_1} + \left(p_{25}s^5 + p_{24}s^4 + p_{23}s^3 + p_{22}s^2 + p_{21}s\right)e^{-s\tau_2}$,

$R(s) = (r_1 s + r_0)\, e^{-s\tau_1} e^{-s\tau_2}$,
where p and r are real coefficients of $P(s)$ and $R(s)$ polynomials without controller parameters (K_P, K_I). The arranged characteristic equation in (2) is further represented as a second-order polynomial as shown below:

$$\Delta(s, \tau_1, \tau_2) = R(s)n^2 + P(s)n + M(s) = 0, \tag{3}$$

where n is an unknown variable defined by $n = (K_P s + K_I)$. By solving for the roots of (3) in terms $M(s), P(s)$, and R(s) with real coefficients, a set of PI controller parameters in the (K_P, K_I)-plane can be calculated using the stability boundary locus approach [16,17]. The unknown roots of the polynomial of (3) are first obtained as follows:

$$n_{1,2} = (K_P s + K_I) = \frac{-P(s) \pm \sqrt{P(s)^2 - 4M(s)R(s)}}{2R(s)}. \tag{4}$$

The boundary locus of the stability region could be calculated by substituting $s = j\omega_c$ $(\omega_c > 0)$ into the roots in (4):

$$(K_P(j\omega_c) + K_I) = \frac{-P(j\omega_c) \pm \sqrt{P(j\omega_c)^2 - 4M(j\omega_c)R(j\omega_c)}}{2R(j\omega_c)}. \tag{5}$$

Please note that polynomials $P(s)$ and $R(s)$ in (2) contain the exponential terms of $e^{-j\omega_c\tau_1}$ and $e^{-j\omega_c\tau_2}$. Substituting $e^{-j\omega_c\tau_i} = \cos(\omega_c\tau_i) - j\sin(\omega_c\tau_i)$, $i = 1, 2$, into polynomials $P(j\omega_c)$ and $R(j\omega_c)$ in (5) and separating the imaginary and real parts, the following equation is determined:

$$\begin{aligned} &K_P A(\omega_c) + K_I B(\omega_c) + \Re\left\{P(\omega_c) \mp \sqrt{P(\omega_c)^2 - 4M(\omega_c)R(\omega_c)}\right\} + \\ &j\left[K_P D(\omega_c) + K_I F(\omega_c)\right] + \Im m\left\{P(\omega_c) \mp \sqrt{P(\omega_c)^2 - 4M(\omega_c)R(\omega_c)}\right\} = 0, \end{aligned} \tag{6}$$

where $\Im m\{\bullet\}$ and $\Re\{\bullet\}$ represent the imaginary and real parts of its argument. By equating the real and imaginary parts of (6) to zero, the following two equations are found in terms of PI controller parameters, incommensurate time delays, and the crossing frequency of $s = j\omega_c$:

$$\begin{aligned} K_{Pi}A(\omega_c) + K_{Ii}B(\omega_c) + C_{1i}(\omega_c) = 0,\\ K_{Pi}D(\omega_c) + K_{Ii}E(\omega_c) + F_{1i}(\omega_c) = 0,\\ i = 1, 2, \end{aligned} \tag{7}$$

where:

$$\begin{aligned} A(\omega_c) &= 2r_0\omega_c \sin(\omega_c\tau_1 + \omega_c\tau_2) - 2r_1\omega_c^2 \cos(\omega_c\tau_1 + \omega_c\tau_2),\\ B(\omega_c) &= 2r_0 \cos(\omega_c\tau_1 + \omega_c\tau_2) + 2r_1\omega_c \sin(\omega_c\tau_1 + \omega_c\tau_2),\\ D(\omega_c) &= 2r_0\omega_c \cos(\omega_c\tau_1 + \omega_c\tau_2) + 2r_1\omega_c^2 \sin(\omega_c\tau_1 + \omega_c\tau_2),\\ E(\omega_c) &= -2r_0 \sin(\omega_c\tau_1 + \omega_c\tau_2) + 2r_1\omega_c \cos(\omega_c\tau_1 + \omega_c\tau_2),\\ C_{1i}(\omega_c) &= \Re\left\{P(\mathrm{j}\omega_c) \mp \sqrt{P(\mathrm{j}\omega_c)^2 - 4M(\mathrm{j}\omega_c)R(\mathrm{j}\omega_c)}\right\},\\ F_{1i}(\omega_c) &= \Im m\left\{P(\mathrm{j}\omega_c) \mp \sqrt{P(\mathrm{j}\omega_c)^2 - 4M(\mathrm{j}\omega_c)R(\mathrm{j}\omega_c)}\right\}. \end{aligned}$$

In the (K_P, K_I)–plane, two stability boundary loci $\ell(K_P, K_I, \omega_c)$ are obtained by simultaneously solving the two equations of (7) for each root in (4):

$$\begin{gathered} K_{Pi} = \frac{B(\omega_c)F_{1i}(\omega_c) - E_1(\omega_c)C_{1i}(\omega_c)}{A_1(\omega_c)E_1(\omega_c) - B_1(\omega_c)D_1(\omega_c)}, \\ K_{Ii} = \frac{D_1(\omega_c)C_{1i}(\omega_c) - A_1(\omega_c)F_{1i}(\omega_c)}{A_1(\omega_c)E_1(\omega_c) - B_1(\omega_c)D_1(\omega_c)}, \\ i = 1, 2. \end{gathered} \tag{8}$$

With the help of (8), stability regions corresponding to each root given in (4) are determined. It is to be noted that the boundaries of these stability regions have to be extracted. These boundaries are known as complex root boundaries (CRBs), as complex roots are crossing the imaginary axis [17]. In addition to these stability boundaries, some roots of (2) can cross the $j\omega$-axis through the origin. As seen from (7) and (8), this crossing of roots will happen only for $K_I = 0$ since the term of $B(\omega_c = 0) \neq 0$ in (7) while all other terms are zero for $\omega_c = 0$, $A(\omega_c) = C_{1i}(\omega_c) = D(\omega_c) = E(\omega_c) = F_{1i}(\omega_c) = 0$. This stability boundary is known as a real root boundary (RRB) [17]. These CRB and RRB loci divide the (K_P, K_I)–plane into unstable and stable regions of the LFC system with incommensurate time delays.

4. Results

In this section, the stability boundary locus is computed by the proposed method in [16,17] for incommensurate time delays in each control area using (8). The verification of the results obtained is validated by both time-domain simulations and the QPmR algorithm. Two-area LFC system parameters are given in the Table.

Table 1. Two-area LFC system parameters [3,6].

Parameters	$T_{ch}(s)$	$T_g(s)$	R	D	β	M
Area 1	0.3	0.1	0.05	1.0	21.0	10.0
Area 2	0.4	0.17	0.05	1.5	21.5	12.0
T_{12}=0.0796 pu						

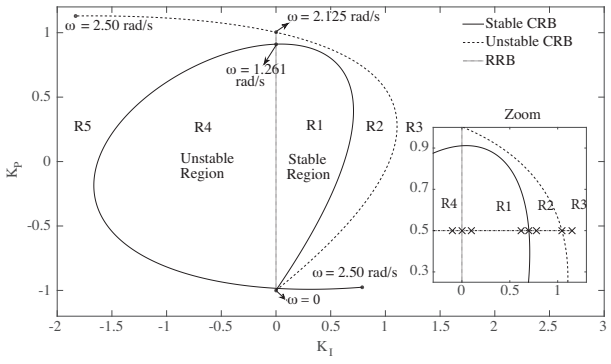

Figure 3. Stable and unstable CRB loci for $|\tau| = 2s$, $\theta = 15^0$.

$|\tau| = 2s$ and $\theta = 15^0$ are first chosen and thereby time delays for areas 1 and 2 are calculated as $\tau_1 = 1.9318s$ and $\tau_2 = 0.5176s$ using the equations of $|\tau|\cos(\theta)$ and $|\tau|\sin(\theta)$, respectively. Stability regions for the desired crossing frequency in the range of $\omega_c \in [0, 2.50]\, rad/s$ are determined in the (K_P, K_I)–plane

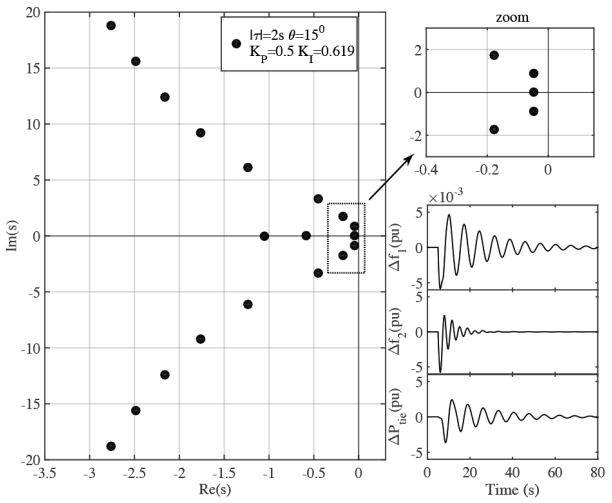

(a) $K_P = 0.5,\ K_I = 0.619$

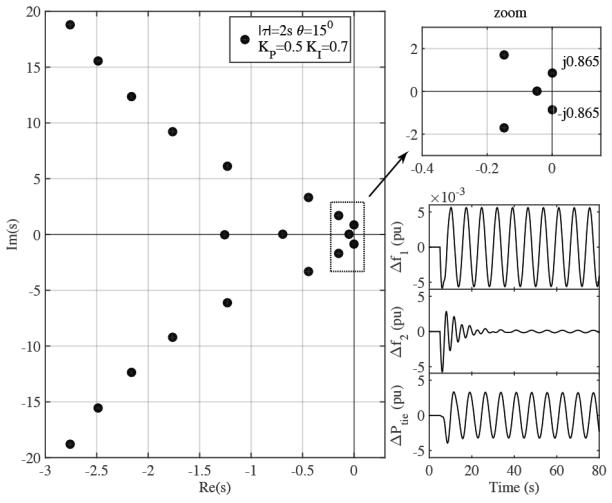

(b) $K_P = 0.5,\ K_I = 0.7$

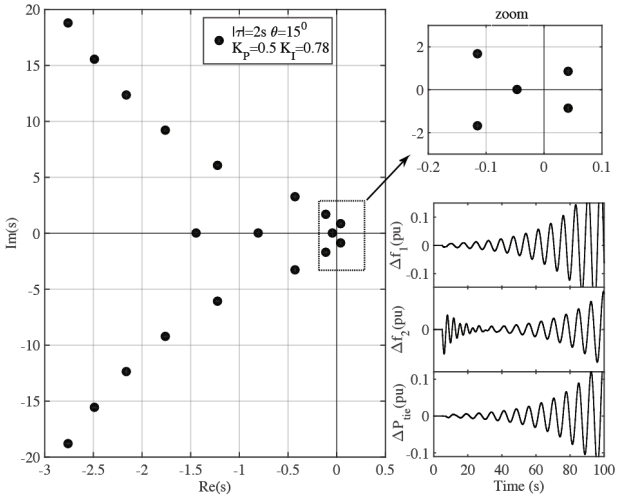

(c) $K_P = 0.5,\ K_I = 0.78$

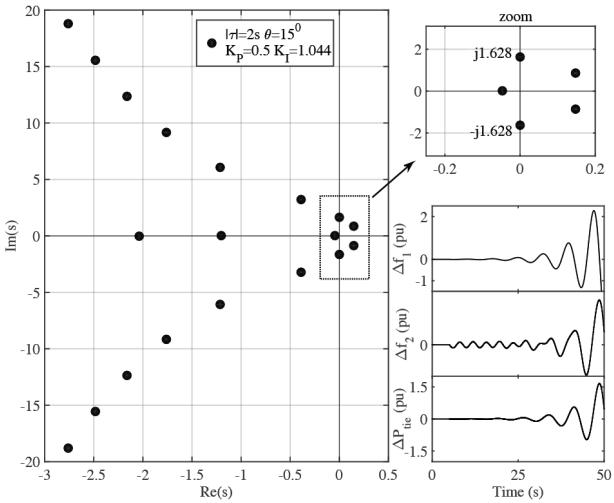

(d) $K_P = 0.5,\ K_I = 1.044$

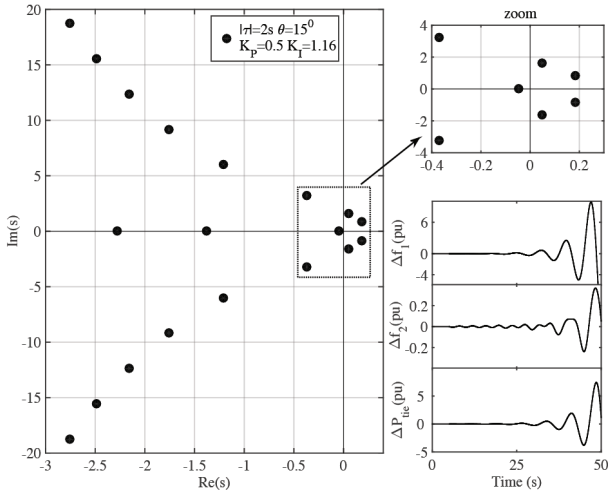

(e) $K_P = 0.5,\ K_I = 1.16$

Figure 4. Dominant roots distribution and dynamic responses for two-area LFC system.

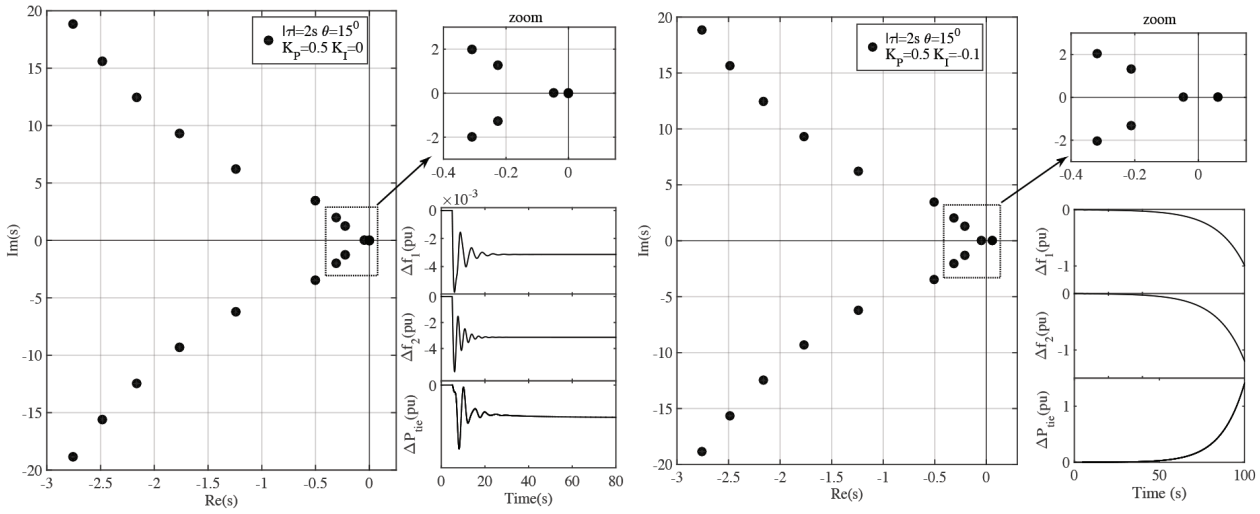

(a) $K_P = 0.5,\ K_I = 0$ (b) $K_P = 0.5,\ K_I = -0.1$

Figure 5. Dominant roots distribution of two-area LFC system for PI controller gains to the left of RRB.

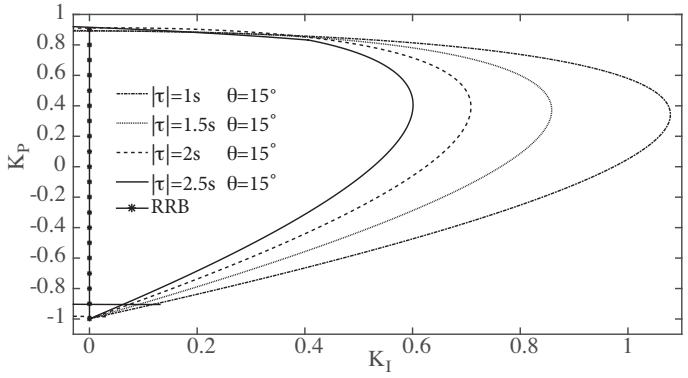

Figure 6. Impact of different time delays on stability regions for fixed $\theta = 15^0$.

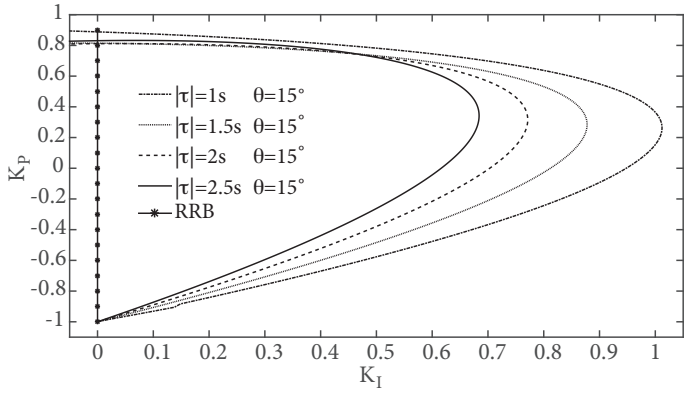

Figure 7. Impact of different time delays on stability regions for fixed $\theta = 45^0$.

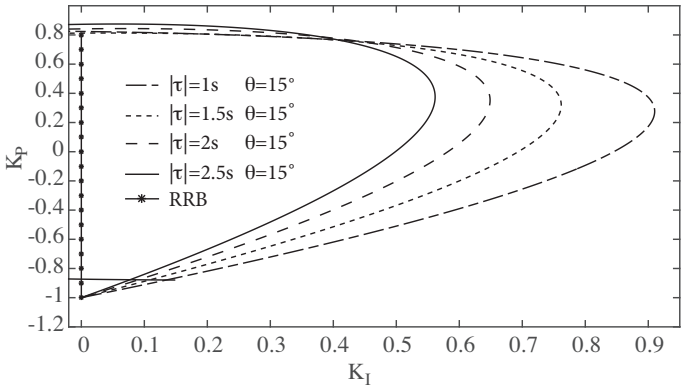

Figure 8. Impact of different time delays on stability regions for fixed $\theta = 75^0$.

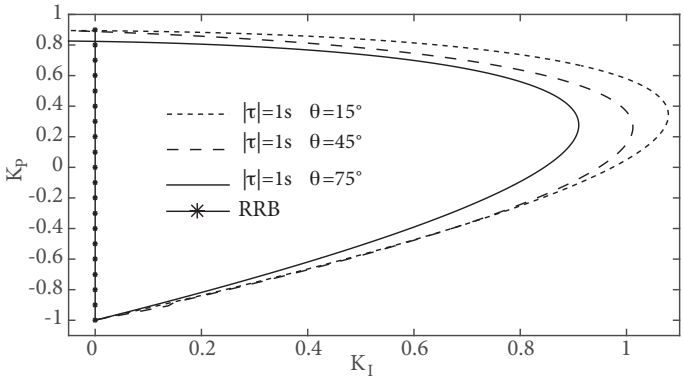

Figure 9. Impact of angle θ on stability region for $|\tau| = 1s$.

and demonstrated in Figure 3. Two CRBs denoted by the solid and dashed lines in Figure 3 are illustrated and the RRB locus is determined by $K_I = 0$. Figure 3 also separates the regions called R1, R2, R3, R4, and R5 to verify the accuracy of the computed stability regions and investigate the LFC system response for the selected $(\theta, |\tau|)$. All roots of the two-area LFC system for any PI controller gains inside region R1 that provide a set of PI controller parameters lie in the left half plane. Figure 4a shows dominant roots' distribution determined by the QPmR algorithm and time-domain simulations in frequency and tie-line power exchange deviation for $K_P = 0.5$, $K_I = 0.619$ in stable region R1. It is clear that there are oscillations in frequency and tie-line power exchange deviation decay, indicating the stability. A pair of complex conjugate roots of the LFC system will be located on the imaginary axis for PI controller gains ($K_P = 0.5$, $K_I = 0.7$) chosen on the stable CRB as shown in Figure 3. It is seen from Figure 4b that the LFC system is marginally stable due to undamped responses for $K_P = 0.5$, $K_I = 0.7$, except for the frequency response of area 2 shown in the middle of the three time-domain simulations. Figure 4c depicts the dominant roots' distribution and the dynamic responses for $K_P = 0.5$, $K_I = 0.78$ in region R2. The system will be unstable due to growing oscillations of the system responses and a pair of complex roots located in the right half of the complex plane as seen from Figure 4c. For any PI controller gains ($K_P = 0.5$, $K_I = 1.044$) selected on the unstable CRB described in Figure 3, another pair of complex roots of the characteristic equation(2) will be on the imaginary axis as shown in Figure 4d. It is clear that the LFC system is unstable from Figure 4d. The LFC system also has two additional roots in the

right half of the complex plane from dominant roots' distribution for $K_P = 0.5$, $K_I = 1.16$ outside the unstable CRB, in region R3. The instability of the system for the given PI controller gains is clearly shown in Figure 4e. Furthermore, recall that $K_I = 0$ is the RRB locus. The dynamic response of the LFC system around RRB is investigated. It can be seen from (2) that the LFC system has a root at the origin ($K_I = 0$) defining the RRB locus and all other dominant roots of the two-area LFC system are located in the left half plane. Figure 5a illustrates that the LFC system is stable for $K_P = 0.5$, $K_I = 0$. For all PI controller parameters, the system will have a stable response due to a root at the origin on the RRB locus. Moreover, the LFC system has a real positive root for any PI controller parameters to the left of the $K_I = 0$ line, as depicted from the dominant roots' distribution in Figure 5a. Therefore, the LFC system exhibits exponential or nonoscillatory instability in region R4 shown by time-domain simulations in the aforementioned Figure 5b. Likewise, Figure 3 shows the exponential instability of the LFC system for any PI controller gains of region R5. Finally, similar to region R2, region R5 in Figure 3 presents the set of PI controller parameters for which the LFC system is oscillatory unstable.

$|\tau|$ and θ are two important parameters used for the identification of stability regions. Recall that the selection of incommensurate delays (τ_1, τ_2) is achieved by using the polar coordinates and the values of (τ_1, τ_2) are specified by choosing $|\tau|$ and θ as described in Figure 2. The effect of $|\tau|$ on the stability regions is first investigated for three different cases mentioned in Section 3.1. Case 1, Case 2, and Case 3 correspond to $\theta = 15^0$ $(\tau_1 > \tau_2\ ,\ 0^0 \leq \theta < 45^0)$, $\theta = 45^0$ $(\tau_1 = \tau_2\ ,\ \theta = 45^0)$, and $\theta = 75^0$ $(\tau_1 < \tau_2\ ,45^0 < \theta \leq 90^0)$, respectively. The magnitude $|\tau|$ for each case is selected as $1s$, $1.5s$, $2s$, and $2.5s$. The stability regions for $\theta = 15^0$ $(\tau_1 > \tau_2)$ are obtained and shown in Figure 6. Time delay values (τ_1, τ_2) corresponding to $\theta = 15^0$ for Case 1 are computed as $(0.969s, 0.259s)$, $(1.449s, 0.388s)$, $(1.932s, 0.518s)$, and $(2.415s, 0.647s)$, respectively. As the magnitude of $|\tau|$ increases, stability regions are becoming smaller, as seen from Figure 6. Next, the stability regions obtained for Case 2 $(\theta = 45^0, \tau_1 = \tau_2)$ and Case 3 $(\theta = 75^0, \tau_1 < \tau_2)$ are illustrated in Figure 7 and 8, respectively. Similar to the results presented in Figure 6, an increase in the delay magnitude $|\tau|$ results in decrease of size of the stability regions for both Case 1 and Case 2. As a result, Figures 6, 7, and 8 indicate that the stability regions shrink for each case defined by $\theta \in [0^0 - 45^0)$, $\theta = 45^0$, and $\theta \in (45^0 - 90^0]$ when magnitude $|\tau|$ is increased for fixed θ. Furthermore, the impact of angle θ on stability regions is investigated when the magnitude of $|\tau|$ is kept constant. Figure 9 depicts stability regions for $\theta = 15^0, 45^0$, and 75^0 when the magnitude of the delay is fixed at $|\tau| = 1s$. As seen from Figure 9, the size of stability regions decreases when angle θ is increased for $\theta \in [15^0 - 75^0]$. Also, it is clear from Figure 9 that the largest of PI controller sets is obtained for Case 1, in which τ_1 is greater than τ_2 $(\tau_1 > \tau_2)$. Figure 9 clearly illustrates that the size of the regions is significantly affected by the incommensurate time delays in each control area. For example, the region becomes larger when the delay in area 1 is greater than that of area 2 as compared to the case of two identical delays in each region $(\tau_1 = \tau_2)$. On the other hand, the stability region shrinks for Case 3, in which the time delay in area 1 is less than that of area 2 $(\tau_1 < \tau_2)$.

5. Conclusions

This paper has presented the implementation of a stability boundary locus method to determine all stabilizing PI controller parameters that constitute a stability region in the PI controller parameter space for two-area LFC systems with multiple incommensurate time delays. Stability regions have been determined for different delay variation scenarios. The size of the regions is significantly affected by the incommensurate time delays

as compared with the identical time delay case in each control area. Furthermore, it is clearly seen from the results that the largest PI controller set is obtained for the delay case in which the delay for area 1 is greater than the delay for area 2. Results indicate that incommensurate delays need to be taken into account in the computation of stability regions for a realistic PI controller design of LFC systems.

Clearly, in addition to the stability, other performance criteria such as gain and phase margins, maximum overshoot, a fast dynamic response, and smaller settling time in the frequency deviation could be considered and an optimal subset of PI controller parameters inside the stability region could be identified. With the help of various soft optimization techniques including genetic algorithms or particle swarm optimization, stability regions could be optimized and thus proper PI controller parameter values ensuring a good dynamic performance could be computed. As future work, different optimization techniques will be implemented to identify a subset of optimal PI controller parameters inside stability regions.

References

[1] Kundur P. Power System Stability and Control. New York, NY, USA: McGraw-Hill, 1994.

[2] Liu S, Liu PX, Wang X. Stability analysis and compensation of network-induced delays in communication-based power system control: a survey. ISA Transactions 2017; 66: 143–153. doi: 10.1016/j.isatra.2016.09.022

[3] Yu X, Tomsovic K. Application of linear matrix inequalities for load frequency control with communication delays. IEEE Transactions on Power Systems 2004; 19 (3): 1508-1515. doi: 10.1109/TPWRS.2004.831670

[4] Mohammadi L, Alfi A. Guaranteed cost control in delayed teleoperation systems under actuator saturation. Iranian Journal of Science and Technology, Transactions of Electrical Engineering (in press). doi: 10.1007/s40998-019-00206-6

[5] Ghaleh HS, Alfi A. Bilateral control of uncertain telerobotic systems using iterative learning control: design and stability analysis. Acta Astronautica 2019; 156: 58-69. doi: 10.1016/j.actaastro.2018.07.043

[6] Sönmez Ş, Ayasun S, Nwankpa CO. An exact method for computing delay margin for stability of load frequency control systems with constant communication delays. IEEE Transactions on Power Systems 2016; 31 (1): 370-377. doi: 10.1109/TPWRS.2015.2403865

[7] Liu M, Yang L, Gan D, Wang D, Gao F et al. The stability of AGC systems with commensurate delays. International Transactions on Electrical Energy Systems 2007; 17 (6): 615-627. doi: 10.1002/etep.159

[8] Walton KE, Marshall JE. Direct method for TDS stability analysis. IEE Proceedings Part D 1987; 134 (2): 101–107. doi: 10.1049/ip-d.1987.0018

[9] Gündüz H, Sönmez Ş, Ayasun S. Comprehensive gain and phase margins based stability analysis of micro-grid frequency control system with constant communication time delay. IET Generation, Transmission and Distribution 2017; 11 (3): 719-729. doi: 10.1049/iet-gtd.2016.0644

[10] Rekasius ZV. A stability test for systems with delays. In: Joint Automatic Control Conference; San Francisco, CA, USA; 1980. Paper No. TP9-A.

[11] Olgac N, Sipahi R. An exact method for the stability analysis of time-delayed linear time-invariant (LTI) systems. IEEE Transactions on Automatic Control 2002; 47 (5): 793-797. doi: 10.1109/TAC.2002.1000275

[12] Sönmez Ş, Ayasun S, Eminoğlu U. Computation of time delay margins for stability of a single-area load frequency control system with communication delay. WSEAS Transactions on Power Systems 2016; 9: 67-76.

[13] Jiang L, Yao W, Wu QH, Wen, JY, Cheng SJ. Delay-dependent stability for load frequency control with constant and time-varying delays. IEEE Transactions on Power Systems 2012; 27 (2): 932-941. doi: 10.1109/TPWRS.2011.2172821

[14] Zhang CK, Jiang L, Wu QH, He Y, Wu M. Further results on delay-dependent stability of multi-area load frequency control. IEEE Transactions on Power Systems 2013; 28 (4): 4465-4474. doi: 10.1109/TPWRS.2013.2265104

[15] Krishnan R, Pragatheeswaran JK, Ray G. Robust stability of networked load frequency control systems with time-varying delays. Electric Power Components and Systems 2017; 45 (3): 302–314. doi: 10.1080/15325008.2016.1248249

[16] Söylemez MT, Munro N, Baki H. Fast calculation of stabilizing PID controller. Automatica 2003; 39 (1): 121–126. doi: 10.1016/S0005-1098(02)00180-2

[17] Tan N, Kaya I, Yeroglu C, Atherton DP. Computation of stabilizing PI and PID controllers using the stability boundary locus. Energy Conversion and Management 2006; 47(18-19): 3045-3058. doi: 10.1016/j.enconman.2006.03.022

[18] Hamamcı SE, Tan N. Design of PI controllers for achieving time and frequency domain specifications simultaneously. ISA Transactions 2006; 45 (4): 529-543. doi: 10.1016/S0019-0578(07)60230-4

[19] Hamamcı SE, Köksal M. Calculation of all stabilizing fractional-order PD controllers for integrating time delays. Computers and Mathematics with Applications 2010; 59 (5): 1621-1629. doi: 10.1016/j.camwa.2009.08.049

[20] Wang J, Tse N, Gao Z. Synthesis on-PI-based pitch controller of large wind turbine generator. Energy Conversion and Management 2011; 52 (2): 1288-1294. doi: 10.1016/j.enconman.2010.09.026

[21] Melchor-Aguilar D, Niculescu SI. Computing non-fragile PI controllers for delay models of TCP/AQM networks. International Journal of Control 2009; 82 (12): 2249–2259. doi: 10.1080/00207170902984741

[22] Guel-Cortez AJ, Mendez-Barrios CF, Gonzalez-Galvan EJ, Mejia-Rodriguez G, Felix L. Geometrical design of fractional PD$^{\mu}$ controllers for linear time-invariant fractional-order systems with time delay. Journal of Systems and Control Engineering(in press). doi: 10.1177/0959651818823450.

[23] Sönmez Ş, Ayasun S. Stability region in the parameter space of PI controller for a single-area load frequency control system with time delay. IEEE Transactions on Power Systems 2016; 31 (1): 829-830. doi: 10.1109/TPWRS.2015.2412678

[24] Sönmez Ş, Ayasun S. Gain and phase margins based delay-dependent stability analysis of single-area load frequency control system with constant communication time delay. Transactions of the Institute of Measurement and Control 2018; 40 (5): 1701-1710. doi: 10.1177/0142331217690221

[25] Sönmez Ş, Ayasun S. Computation of PI controllers ensuring desired gain and phase margins for two-area load frequency control system with communication time delays. Electric Power Components and Systems 2018; 46 (8): 938-947. doi: 10.1080/15325008.2018.1509914

[26] Vyhlídal T, Zítek P. Mapping based algorithm for large-scale computation of quasi-polynomial zeros. IEEE Transactions on Automatic Control 2009; 54 (1): 171-177. doi: 10.1109/TAC.2008.2008345

[27] MathWorks Inc. Model-Based and System-Based Design, Using Simulink. Natick, MA, USA: MathWorks, 2000.

[28] Vyhlídal T, Olgaç N, Kučera V. Delayed resonator with acceleration feedback – complete stability analysis by spectral methods and vibration absorber design. Journal of Sound and Vibration 2014; 333 (25): 6781–6795. doi: 10.1016/j.jsv.2014.08.002

[29] Kammer AS, Olgaç N. Delayed-feedback vibration absorbers to enhance energy harvesting. Journal of Sound and Vibration 2016; 363 (17): 54–67. doi: 10.1016/j.jsv.2015.10.030

[30] Zhu Q, Jiang L, Yao W, Zhank CK, Luo C. Robust load frequency control with dynamic demand response for deregulated power systems considering communication delays. Electric Power Components and Systems 2017; 45 (1): 75-87. doi: 10.1080/15325008.2016.1233300